09

Polarization effects electromagnetically induced transparency in the Λ-scheme of degenerated levels

© O.M. Parshkov

Yuri Gagarin State Technical University of Saratov,
410054 Saratov, Russia
e-mail: oparshkov@mail.ru

Received December 18, 2024
Revised December 18, 2024
Accepted December 18, 2024

The conclusions of a theoretical study of the phenomenon of electromagnetic induced transparency with elliptical polarization of probe and control pulses are reported. The resonant medium is modeled by the Λ-scheme of degenerate transitions between the $^3P_0$, $^3P_1$ and $^3P_2$ levels of the ^{208}Pb isotope. It is assumed that at the entrance to the medium the probe pulse has a significantly lower intensity and duration than the control field pulse. It is shown that in the medium the probe pulse splits into two elliptically polarized pulses propagating independently of each other. The major axis of the polarization ellipse of one of them is parallel, and the second is perpendicular to the major axis of the polarization ellipse of the control radiation. The speed of movement of a pulse of the second type is significantly less than the speed of propagation of pulses of the first type. Both of these speeds, due to the phenomenon of electromagnetically induced transparency, are significantly less than the speed of light in a vacuum, As the probe field propagates in the medium, its components shifts toward the trailing edge of the control pulse. Reducing the intensity of the control field in the area where the components of the probe radiation are located reduces the effectiveness of the phenomenon of electromagnetic induced transparency. This leads to an increase in the energy loss of the probe radiation and its attenuation. Due to the fact that pulses of the second type have a lower propagation speed, they fall into the region of the trailing edge of the control pulse earlier than pulses of the first type. Therefore, a pulse of the second type penetrates into the medium at a shorter distance than a pulse of the first type.

Keywords: electromagnetically induced transparency, normal modes.

DOI: 10.61011/TP.2025.05.61130.442-24

Introduction

Destructive interference of the probabilities amplitudes of quantum transitions between energy levels during resonant excitation of the medium by coherent laser radiation leads to a number of important effects, a special place among which belongs to the phenomenon of electromagnetically induced transparency (EIT) [1–3]. EIT research has served the basis for the key practical applications, such as creation of optical memory systems [2] and quantum communications [2,4,5], quantum information systems [1–3], devices for precise measurement of magnetic fields [6], devices for precise time measurement [7]. The use of EIT phenomenon allows creating large optical nonlinearities [3,8] and implementing enhanced radiation without populations inversion [9]. The features of EIT have been studied in the correlated quantum gases [10], in the radio band [11], on impurities in photonic crystals [12], near nanofibers [13], and in a test field with orbital angular momentum [14], in terahertz metamaterial [15], on quasi-bound states in continuum [16].

The phenomenon of EIT in case of degenerated energy levels leads to a number of effects related to the polarization characteristics of interacting radiation. In [17,18], the EIT-associated rotation of the probe field polarization plane was theoretically and experimentally studied for the case of change in the control radiation intensity, and in [19,20], the influence of a permanent magnetic field on the evolution of the probe radiation circular components was theoretically and experimentally studied. Linear and circular birefringence of a probe field under EIT was studied theoretically and experimentally in [21]. The possibility of propagation of a probe field in the form of two modes with different polarization states was predicted theoretically in [22] .

[23,24] outlines the findings of theoretical studies of birefringence which goes along with EIT during elliptic polarization of the probe and control fields at the entrance of resonance medium. The studies in these papers were limited by the assumption of the stationary nature of the input control radiation. These studies outlined the Λ-scheme of quantum transitions between the degenerated energy levels $^3P_0$, $^3P_2$, $^3P_1^0$ of isotope ^{208}Pb. In pairs of this isotope the EIT of elliptic polarized laser pulses were observed [25,26]. It was shown by analytical methods in [23,24] that a probe pulse in a medium can be represented as a sum of elliptically polarized normal modes propagating independently of each other.

The assumption of the control field stationarity excludes from consideration the situations often realized in practice when EIT is initiated by short laser pulses.. The following report presents the results of a theoretical study of EIT

phenomenon at the same quantum transitions as in the paper [23], but provided that the control field is pulsed.

1. Setting the boundary value problem

The reviewed Λ-scheme consisting of the non-degenerate lower level $^3P_0$, five-times degenerate medium level $^3P_2$ and a three-time non-degenerate upper level $^3P_1^0$ is given in Fig. 1. The level $^3P_1$ is associated with the upper and middle levels of Λ-scheme by means of electro-dipole moments, but not included in Λ-scheme. The values ω_1 and ω_2 represent the natural central frequencies of inhomogeneously broadened quantum transitions. Relaxation processes connecting the excited levels of Λ-scheme with the level $^3P_1$ lead to a decrease in the total number of atoms at its levels and an additional broadening of spectral lines.

Let's assume ϕ_k $(k = 1, 2, \ldots, 9)$ — an orthonormal set of general eigen functions of Hamilton operators, the square of the angular momentum, and the projection of the angular momentum onto the axis z. Function ϕ_1 describes the state $^3P_0$ $(M = 0)$, functions ϕ_k $(k = 5, 6, \ldots, 9)$ relate to the states $^3P_2$ $(M = -2, -1, 0, 1, 2)$ respectively, and functions ϕ_k $(k = 2, 3, 4)$ — respectively, correspond to the states $^3P_1^0$ $(M = -1, 0, 1)$ (Fig. 1). Let's assume D_1 and D_2 — the given reduced electrodipole moments of transitions $^3P_0 \to {}^3P_1^0$ and $^3P_2 \to {}^3P_1^0$ respectively, while ω_1 and ω_2 $(\omega_1 > \omega_2)$ — frequencies of these transitions for the resting atom. Given the resonance medium is itself a rarefied gas, let's introduce the designation $T_1 = 2/\Delta_1$, where Δ_1 — width (by level of e^{-1} height) density

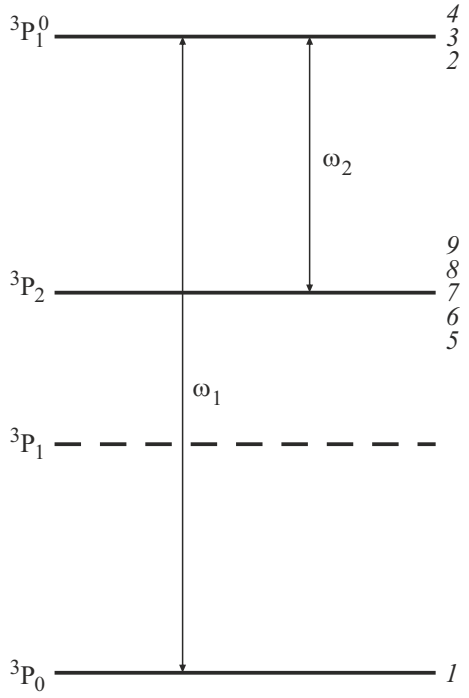

Figure 1. Energy levels of Λ-scheme (continuous lines); digits on the right of the level line — the numbers of states relating to this level according to the theoretical model.

of distribution $g(\omega_1')$ of frequencies ω_1' of the quantum transition $^3P_0 \to {}^3P_1^0$ because of Doppler effect

$$g(\omega_1') = \left(T_1/\sqrt{\pi}\right)\exp\left[-T_1^2(\omega_1' - \omega_1)^2\right].$$

The electric field strength of two laser pulses propagating along the z axis is represented as $\mathbf{E} = \mathbf{E}_1 + \mathbf{E}_2$, where

$$\mathbf{E}_l = \mu_l\left[\mathbf{i}E_{xl}\cos(\omega_l t - k_l z + \delta_{xl}) + \mathbf{j}E_{yl}\cos(\omega_l t - k_l z + \delta_{yl})\right],$$

$$l = 1, 2. \qquad (1)$$

Here $\mathbf{E}_l$ and ω_l — strength of electrical field and radiation frequency carrier, $\mathbf{i}$ and $\mathbf{j}$ — axis-unit vectors x, y; E_{xl}, E_{yl} — amplitudes x and y of the fields components. The values δ_{xl}, δ_{yl} describe the phase modulation of these components, $\mu_l = \hbar\sqrt{2l+1}/(|D_l|T_1)$, $k_l = \omega_l/c$. According to EIT theory terminology, at $l = 1$ formula (1) describes the probe radiation and at $l = 2$ – control radiation [1–3].

Let's define the values f_l and g_l by equalities

$$f_l = \left[E_{xl}\exp(i\delta_{xl}) - iE_{yl}\exp(i\delta_{yl})\right]/\sqrt{2},$$

$$g_l = \left[E_{xl}\exp(i\delta_{xl}) + iE_{yl}\exp(i\delta_{yl})\right]/\sqrt{2}. \qquad (2)$$

According to [27], f_l and g_l are called amplitudes of the left-side and right-side circular components of the probe $(l = 1)$ and control $(l = 2)$ fields. Let's present the wave function of the atom as

$$\Psi = \overline{c}_1\phi_1 + \left(\sum_{k=2}^{4}\overline{c}_k\phi_k\right)\exp(-i\xi_1) + \left(\sum_{k=5}^{9}\overline{c}_k\phi_k\right) \times \exp\left[-i(\xi_1 - \xi_2)\right],$$

$(k = 1, 2, \ldots, 9)$ — amplitude indicators of the quantum states populations probability, and $\xi_l = \omega_l t - k_l z$, $l = 1, 2$. Let's denote the values by the following relationships:

$$c_1 = p_1^*\overline{c}_1, \quad c_2 = \overline{c}_2, \quad c_4 = \overline{c}_4, \quad c_5 = p_2\overline{c}_5,$$

$$c_7 = (1/\sqrt{6})p_2\overline{c}_7, \quad c_9 = p_2\overline{c}_9,$$

where $p_l = 2D_l/|D_l|$ $l = 1, 2$. Let's denote the normalized independent variables s and w:

$$s = z/z_0, \quad w = (t - z/c)/T_1; \quad z_0 = 3\hbar c/(2\pi N|D_1|^2 T_1\omega_1),$$

where N — concentration of atoms. Using Maxwell and Schrodinger equations, we obtain the following system of equations in the first approximation of the slow envelope

method:

$$\frac{\partial f_1}{\partial s} = \frac{i}{\sqrt{\pi}} \int_{-\infty}^{+\infty} c_1 c_2^* \exp(-\varepsilon_1^2) d\varepsilon_1,$$

$$\frac{\partial f_2}{\partial s} = -\frac{i}{\sqrt{\pi}} \xi \int_{-\infty}^{+\infty} (c_4^* c_9 + c_2^* c_7) \exp(-\varepsilon_1^2) d\varepsilon_1,$$

$$\frac{\partial g_1}{\partial s} = -\frac{i}{\sqrt{\pi}} \int_{-\infty}^{+\infty} c_1 c_4^* \exp(-\varepsilon_1^2) d\varepsilon_1,$$

$$\frac{\partial g_2}{\partial s} = \frac{i}{\sqrt{\pi}} \xi \int_{-\infty}^{+\infty} (c_2^* c_5 + c_4^* c_7) \exp(-\varepsilon_1^2) d\varepsilon_1,$$

$$\frac{\partial c_1}{\partial w} = -i(f_1 c_2 - g_1 c_4),$$

$$\frac{\partial c_2}{\partial w} + i\varepsilon_1 c_2 = -\frac{i}{4}(f_1^* c_1 + g_2^* c_5 - f_2^* c_7) - \gamma c_2,$$

$$\frac{\partial c_4}{\partial w} + i\varepsilon_1 c_4 = \frac{i}{4}(g_1^* c_1 - g_2^* c_7 + f_2^* c_9) - \gamma c_4,$$

$$\frac{\partial c_5}{\partial w} + i(\varepsilon_1 - \varepsilon_2) c_5 = -i g_2 c_2,$$

$$\frac{\partial c_7}{\partial w} + i(\varepsilon_1 - \varepsilon_2) c_7 = \frac{i}{6}(g_2 c_2 - g_2 c_4),$$

$$\frac{\partial c_9}{\partial w} + i(\varepsilon_1 - \varepsilon_2) c_9 = i f_2 c_4, \qquad (3)$$

where

$$\varepsilon_1 = (\omega_1' - \omega_1)/\Delta_1, \quad \varepsilon_2 = \beta\varepsilon_1,$$

$$\xi = 0.6\beta|D_2/D_1|^2, \quad \beta = \omega_2/\omega_1.$$

The system of equations (3) doesn't contain the amplitudes $\overline{c}_3$, $\overline{c}_6$ and $\overline{c}_8$, which is consistent with the selection rules ($\Delta M = \pm 1$) for transition under the action of circular field components (1). The terms $-\gamma c_2$ and $-\gamma c_4$ are phenomenologically introduced into the equations for c_2 and c_4 to account for the spontaneous decay of the upper-level states of the studied Λ-scheme. Here $\gamma = T_1/(2\tau)$, where τ — radiation time of life of level $^3P_1^0$.

The boundary conditions for the system (3) and results of its solution may be conveniently expressed as parameters a_l, α_l, γ_l of polarization ellipses (PE) of the probe ($l = 1$) and control ($l = 2$) radiation. Here a_l — semi-major axis of PE measured in units μ_l, α_l — angle of its inclination to x axis in radians, γ_l — compression parameter ($0 \le \alpha_l < \pi$, $-1 \le \gamma_l \le +1$). These values as well as one of the variables δ_{xl}, δ_{yl}, unambiguously define the values f_l and g_l expressed from the formulae (2) [27]. It should be noted that $|\gamma_l|$ is equal to the ratio of the minor axis of PE to its major axis, and the polarization is right (left) elliptical at ifx83xe ($\gamma_l > 0$).

The system of equations (3) is supplemented by the boundary conditions

$$a_l = a_{l0}, \quad \alpha_l = \alpha_{l0}, \quad \gamma_l = \gamma_{l0}, \quad \delta_{sl} = \delta_{xl0};$$

$$s = 0, \quad w \ge 0; \quad l = 1, 2. \qquad (4)$$

Here, $a_{l0}, \alpha_{l0}, \gamma_{l0}, \delta_{xl0}$ — functions of w describing the evolution of a_l, α_l, γ_l, δ_{xl} on the input surface $s = 0$ of the resonance medium. It is suggested that in the initial moment of time $w = 0$ all atoms ^{208}Pb are located at the lower energy level of Λ-scheme.

2. Normal modes

In paper [23], the system (3) was simplified under the assumption of a weak probe field compared to the field of control radiation, i.e. when the following condition is fulfilled

$$v = \sqrt{E_{x1}^2 + E_{y1}^2} \Big/ \sqrt{E_{x2}^2 + E_{y2}^2} \ll 1. \qquad (5)$$

The analysis of the system of equations from (3) in the first approximation with respect to a small parameter v resulted in the following conclusions. The pulse of the control field propagates in a medium at the speed of light in a vacuum without changing the shape of the envelope a_2 and its other characteristics. The probe radiation is the sum of normal modes propagating independently of each other. Normal modes are intrinsic elliptically polarized waves. The main axis of the polarization ellipse of one of the normal modes is parallel to the main axis of PE of the control radiation, whereas the main axis of PE of the other normal mode is perpendicular to the latter. These modes are further referred to as parallel and perpendicular modes, respectively.

The compression parameters γ_1 of parallel and perpendicular normal modes are the same in modulus, opposite in sign, and independent of s and w. These values depend only on the compression parameter γ_2 of PE of the input control field. The value γ_1 for the parallel normal mode is found from the ratio

$$\kappa = -p + \sqrt{p^2 + 1}, \quad \kappa = (1 + \gamma_1)/(1 - \gamma_1),$$

$$p = 10\gamma_2/(1 - \gamma_2^2). \qquad (6)$$

This paper describes a technique for representing the probe pulse as a sum of normal modes on the input surface of the medium ($s = 0$). This technique allows expressing the characteristics of each mode, namely the values a_{l0}, α_{l0}, γ_{l0}, δ_{xl0} on the input surface of the medium through the corresponding characteristics of the total input probe pulse.

On the input surface, the pulses of normal modes overlap in time, forming an input probe pulse. However, due to the difference in the propagation velocities of the modes, the pulse of the probe field in the medium splits into two separate pulses representing each normal mode. It should be stressed that values α_{l0}, γ_{l0}, δ_{xl0} for each mode and do not depend on variables w and s.

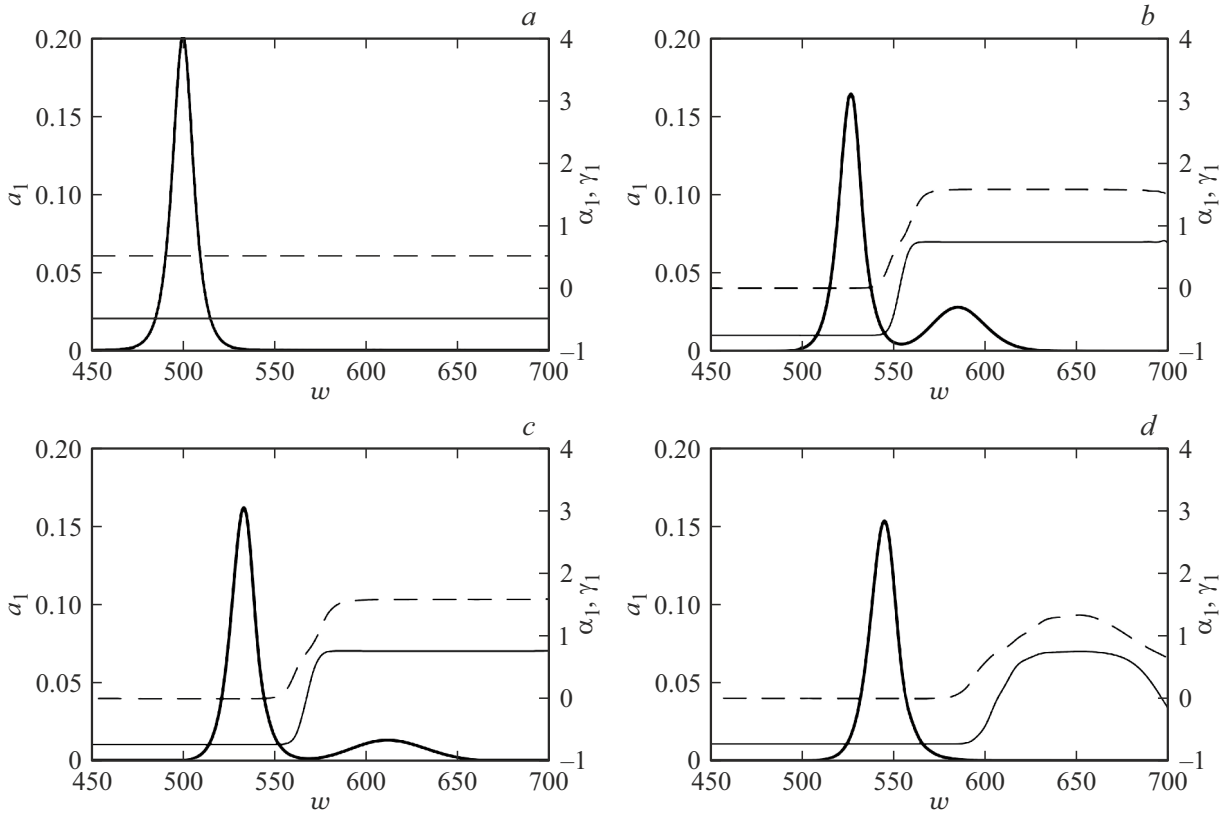

Figure 2. Evolution of values a_1 (thick lines), γ_1 (thin lines) and α_1 (dashes) at $s = 0$ (*a*), 250 (*b*), 300 (*c*), 400 (*d*).

In the mentioned study, it was assumed that all characteristics of PE of the input control field, including the number and values of a_{20}, are constant. This is only possible if continuous laser radiation is used as a control field. However, it is clearly seen that everything said above about normal modes remains true even with the pulsed nature of the control field until condition (5) is fulfilled.

3. Numerical results

The conclusions of the normal mode theory are based on the analysis of the system of equations (3) in the first approximation with respect to a small parameter v (5). To confirm these conclusions and obtain new information about the features of EIT phenomenon, the results of numerical solution of the initial system of equations (3) are given below when specifying the boundary conditions (4).

In the studied Λ-scheme $\beta = 0.7$, $\xi = 2.1$, $\tau = 5.6$ ns [28]. At $T \sim 950-1200$ K the dimensionless unit of time w corresponds to 0.16 ns. The dimensionless unit of distance s significantly depends on temperature. At $T = 1000$ K it corresponds approximately to 0.01 cm, and at $T = 1100$ K it is decreased to about 0.002 cm. The latest estimates are valid for saturated vapors of ^{208}Pb isotope and are based on the data from the reference book [29].

3.1. Opposite directions of the elliptic polarizations of input pulses

Let's define the boundary conditions (4) as follows:

$$a_{10} = 0.2\mathrm{sech}[(w - 500)/5], \quad \alpha_{10} = \pi/6,$$

$$\gamma_{10} = -0.5, \quad \delta_{x10} = 0; \tag{7}$$

$$a_{20} = 6.65\mathrm{sech}[(w - 500)/100], \quad \alpha_{20} = 0,$$

$$\gamma_{20} = 0.3, \quad \delta_{x20} = 0. \tag{8}$$

According to (7) and (8), the magnitudes of the main axes of input fields' PE vary according to the inverse hyperbolic cosine law, and the fields have no phase modulation. The input probe pulse has a right-side elliptic polarization, and the input control pulse has a left-side elliptic polarization. The angle between the large axes of PE of the probe and control fields is equal $\pi/6$.

At $T \sim 1000-1200$ K the duration of the input probe pulse to the level of half the maximal intensity was approximately equal to 1.5 ns, and its peak intensity was about 70 W/cm^2. The duration of the input control pulse to the level of half the maximum intensity is about 30 ns at a peak intensity of about 20 kW/cm^2.

The curves of a_1, α_1 and γ_1 are given in Fig. 2 for the four values of s.

Figure 2 shows that the input probe pulse splits into two pulses in the medium. At $s = 300$ in the region

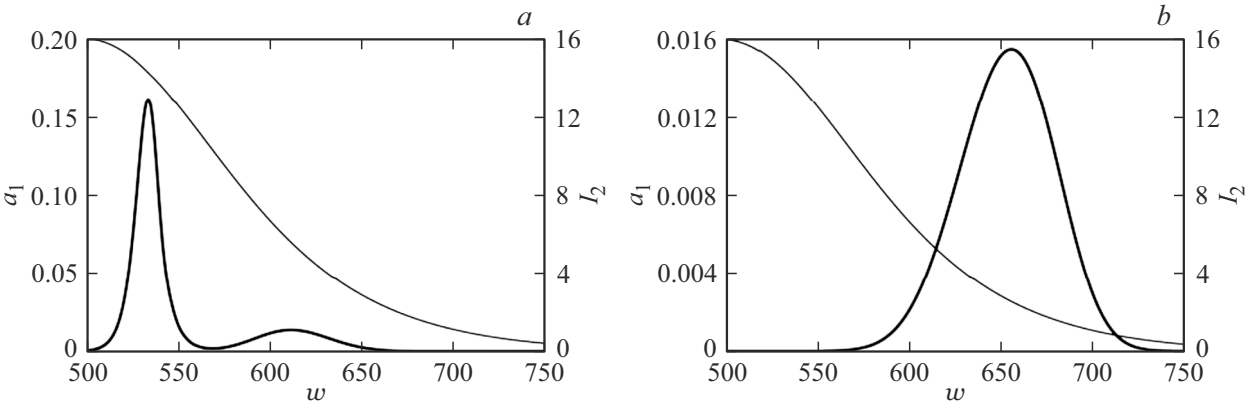

Figure 3. Evolution of values a_1 (thick lines) and I_2 (thin lines) ats = 300 (a) and 940 (b).

where the first of them is located (left-hand pulse) $\alpha_1 = 0$, and in the region where the second one is located (right-hand pulse) $a_1 = \pi/2$. Parameters γ_1 calculated by formulae (6) provides $\gamma_1 = -0.7415$ for the parallel normal mode and $\gamma_1 = 0.7415$ for the perpendicular mode. These values, with an accuracy of three decimal places, coincide with those obtained by numerically solving the system (3) for the first and second pulses in Fig. 2, c, respectively. Therefore, the first pulse is its own parallel normal mode, and the second — is perpendicular to the normal mode. Figure 2 shows that the velocity of propagation of the parallel mode is greater than the velocity of propagation of the perpendicular mode. This was described in [23].

It should be noted that at $s = 400$ in the region $w > 600$ the curve a_1 practically coincides with the abscissa axis. The values of α_1 and γ_1 in this region are not constant. Consequently, at large distances in the range of large values w, the probe radiation does not have properties of the perpendicular normal mode. The parallel normal mode propagates over a much greater distance in the medium and begins to collapse, as will be shown below, at $s > 1500$. The system of equations (3) was solved when replacing in the formulae (8) the boundary condition for a_{20}, corresponding to the pulse nature of the input control field, by condition $a_{20} = 6.65$. The last condition describes continuous input control radiation. Omitting the details of this calculation, we note that in the case of continuous control radiation, both normal modes at a distance of $s = 2000$ lose more than 6% of their energy in the medium.

The reason for the attenuation of modes with a pulsed control field is as follows. When the condition (5) is fulfilled the pulse of control radiation propagates in a medium at the speed of light in the vacuum. The pulses of normal modes have significantly lower propagation velocities. For instance, near the input surface at $T \sim 950$ K the speed of parallel normal mode is about 16 times less than the light speed in vacuum, and the speed of perpendicular mode — is about 40 times less. Therefore the modes pulses are shifted towards the trailing edge of the control pulse. As a result, each of them falls into an area where the intensity of the control field is insufficient for the occurrence of EIT phenomenon. Whereas the process of single-photon resonance interaction of modes with transition between the levels $^3P_0$ and $^3P_1^0$ leads to their fast destruction and decay. The speed of the perpendicular mode is less than that of the parallel mode. Therefore, it first enters the region of a weak control field and penetrates the medium at a shorter distance than the parallel mode.

In Fig. 3 the thick lines indicate the curves of a_1 at distances $s = 300$ and 940. Thin lines denote the curves of intensities I_2 of control radiation measured in units $c\mu_1^2/(8\pi)$. Fig. 3, a corresponds to the distance where maximal value $a_{1m}^{(1)}$ of the quantity a_1 of the perpendicular mode is by order less than the value at $s = 0$. Fig. 3, b corresponds to the distance at which the maximal value $a_{1m}^{(1)}$ of a_1 is decreased by the same number of times for the parallel normal mode. In both cases, as follows from Fig. 3, these modes are detected in the region of small intensity of the control pulse.

The calculation by formulae from [23] demonstrates that parallel normal mode at the input surface ($s = 0$) has the following characteristics:

$$a_{10} = 0.1728\mathrm{sech}[(w - 500)/5], \quad \alpha_{10} = 0,$$
$$\gamma_{10} = -0.7415, \quad \delta_{x10} = 0.2007, \qquad (9)$$

and the perpendicular mode has the following characteristics:

$$a_{10} = 0.0488\mathrm{sech}[(w - 500)/5], \quad \alpha_{10} = \pi/2,$$
$$\gamma_{10} = 0.7415, \quad \delta_{x10} = -1.265. \qquad (10)$$

Fig. 4 shows the curves of a_1, α_1 and γ_1 obtained when solving the system with each of the boundary conditions (9) and (10). Fig. 4, a illustrates that normal modes are overlapped on the input surface. At a distance $s = 250$ (Fig. 4, b) the pulses of modes are spatially separated and the combined graphs of a_1 curves of normal modes practically coincide with the curve a_1 in Fig. 2, b. Also in Fig. 2, b and 4, b the values of α_1 and γ_1 coincide in the regions of location of the appropriate normal modes.

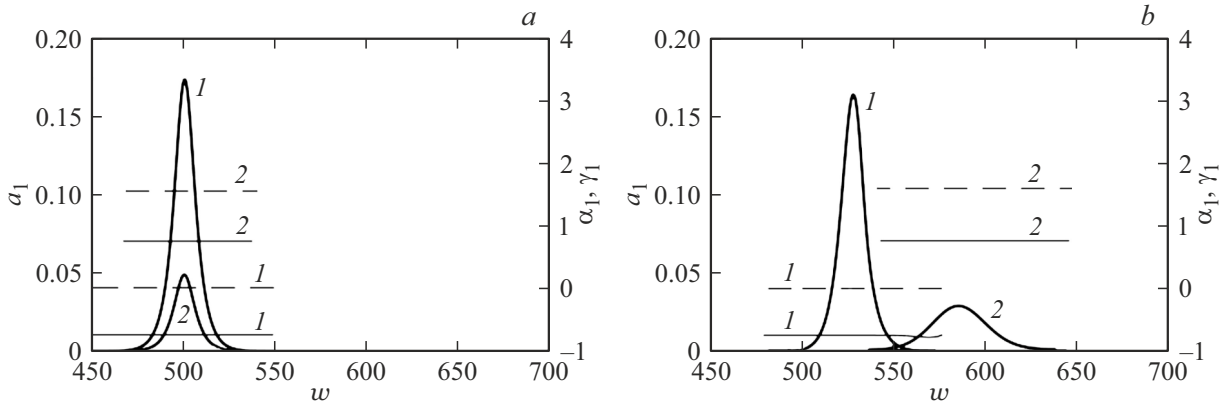

Figure 4. Evolution of values a_1 (thick lines), γ_1 (thin lines) and α_1 (dash) at $s = 0$ (*a*), 250 (*b*); *1* — parallel normal mode, *2* — perpendicular normal mode.

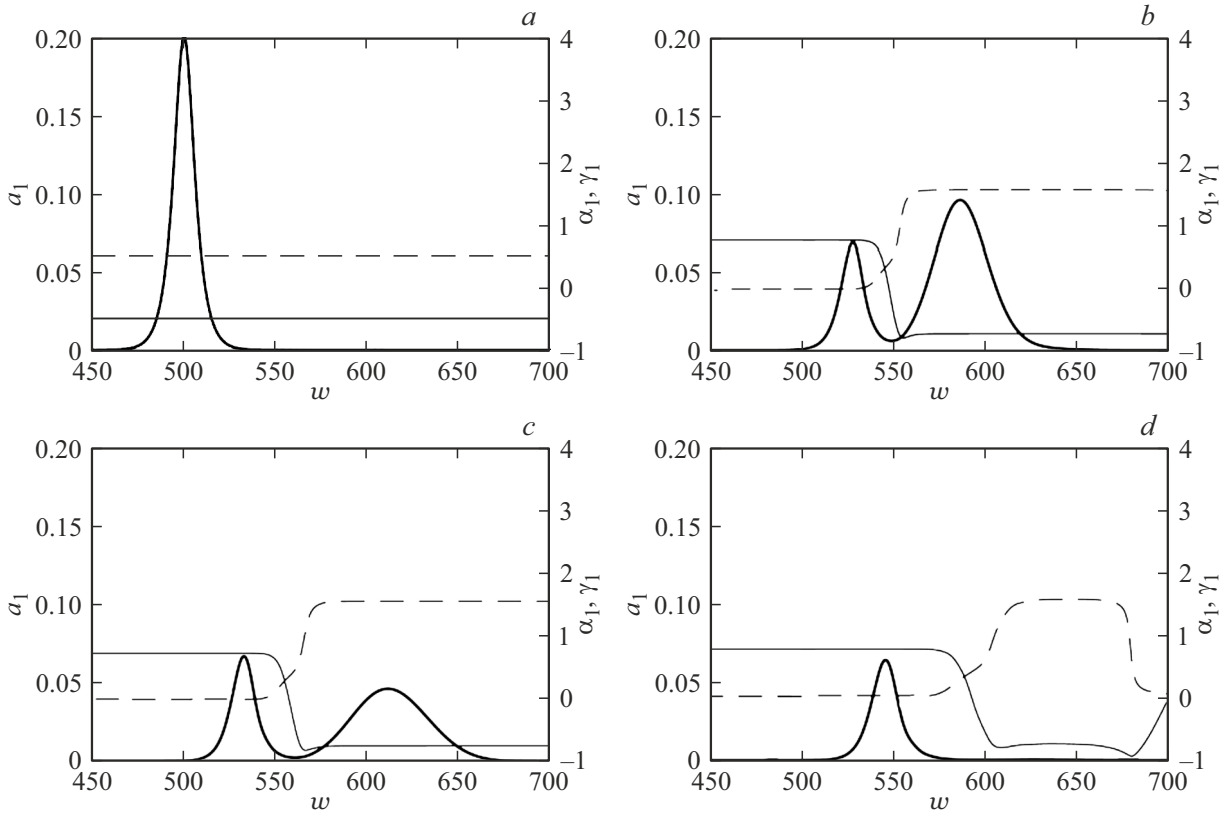

Figure 5. Evolution of values a_1 (thick lines), γ_1 (thin lines) and α_1 (dashes) at $s = 0$ (*a*), 250 (*b*), 300 (*c*), 400 (*d*).

3.2. Identical directions of elliptical polarizations

The boundary conditions for the system of equations (3) now differ from the conditions (7), (8) only by the fact that $\gamma_{20} = -0.3$. In this regard, the input pulses of the probe and control fields have a right-side elliptical polarization. The curves of a_1, α_1 and γ_1 are shown in Fig. 5 for the four values of distance s. On the input surface, the probe pulses have the same characteristics as in the case of different directions of elliptical polarizations of the input fields. Fig. 2 shows that the parallel mode for which $\alpha_1 = 0$ propagates in the medium with a higher speed than the perpendicular mode for which$\alpha_1 = \pi/2$. Near the input surface the condition $a_{1m}^{(1)} < a_{1m}^{(2)}$ is fulfilled (Fig. 5, *b*). Let's bear in mind that in case of different directions of elliptical polarizations of similar fields an opposite situation occurs (Fig. 2, *b*).

The perpendicular mode shifts towards the trailing edge of the control pulse faster than the parallel mode and decays faster in the medium. Therefore, at large distances the ratio

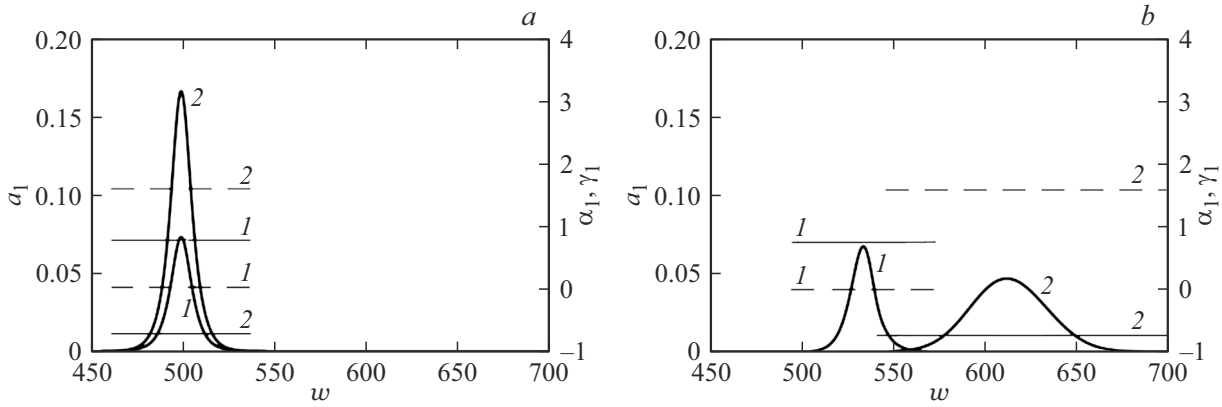

Figure 6. Evolution of values a_1 (thick lines), γ_1 (thin lines) and α_1 (dash) at $s = 0$ (a), 300 (b); *1* — parallel normal mode, *2* — perpendicular normal mode.

$a_{1m}^{(1)} > a_{1m}^{(2)}$ is fulfilled (Fig. 5, c). At a distance of $s = 400$, the perpendicular mode practically disappears (Fig. 5, d), similar to how it happens in the case of different directions of the input fields polarization (Fig. 2, d).

In this situation the parallel mode at $s = 0$ has the following characteristics:

$$a_{10} = 0.0720\mathrm{sech}[(w - 500)/5], \quad \alpha_{10} = 0,$$

$$\gamma_{10} = 0.7415, \quad \delta_{x10} = -0.4990, \qquad (11)$$

and the perpendicular mode has the following characteristics:

$$a_{10} = 0.1645\mathrm{sech}[(w - 500)/5], \quad \alpha_{10} = \pi/2,$$

$$\gamma_{10} = -0.7415, \quad \delta_{x10} = 0.2865. \qquad (12)$$

Fig. 6 shows the curves of a_1, α_1 and γ_1 obtained when solving the system (3) with each of the boundary conditions (11) and (12). Fig. 6, a illustrates that condition $a_{1m}^{(1)} < a_{1m}^{(2)}$ is fulfilled on the input surface. Note that, according to Fig. 4, a, the opposite situation occurs in case of different directions of circular polarizations. In this regard, at a distance of $s = 400$, the pulse of the parallel mode with the same directions of elliptical polarizations of the input fields has a lower height than in case of opposite directions of these polarizations (Fig. 2, d and 5, d).

3.3. Energy of probe radiation

Let us introduce the value $E(s)$, determined by the formula $E(s) = W(s)/W(0)$, where $W(s)$ is the amount of energy transferred by the probe pulse through a unit of cross-sectional area during the entire time it passes through this section. The value $E(s)$ indicates what fraction of the energy of the input probe pulse reaches the distance of s. Curves of $E(s)$ for cases of different (case 1) and identical (case 2) input pulse polarization directions are shown in Fig. 7. The dashed line in Fig. 7 shows a graph of $E(s)$ for case 2 in the absence of relaxation processes, when the decay parameter is $\gamma = 0$.

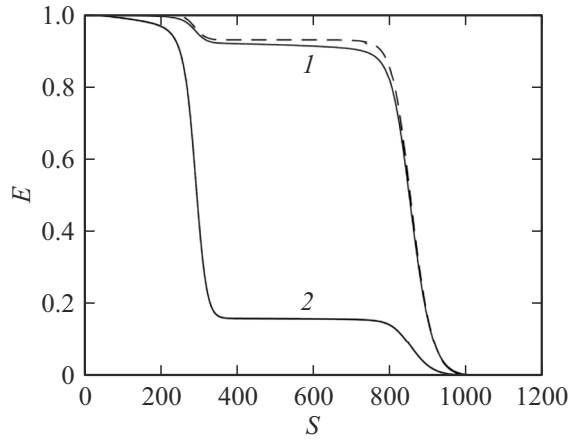

Figure 7. The value E in case 1 (curve *1*) and in case 2 (curve *2*); dash — case 1 if the relaxation processes are absent.

All curves in Fig. 7 are of a stepwise nature. In the initial section of each curve, there is an interval of a slight change in E, followed by a shorter interval of rapid multiplication of this value. For curve *1* it is the interval between approximately the points $s = 250$ and 350, and in case of curve *2* — between the points $s = 200$ and 350. Further, on each curve there are quite long intervals of s axis where the value of E practically doesn't change. At $s > 800$ the values of E rapidly decrease to zero in both cases. At all distances, the value of E for different directions of elliptical polarization of the input fields is greater than in the case of their identical elliptical polarizations.

The above-mentioned features of curves *1* and *2* are of the following nature. Near the input surface, the input probe pulse decays into normal modes. Initially, the modes propagate in conditions favorable for the occurrence of EIT phenomenon and have low energy losses. After that the perpendicular mode falls into the region of the control pulse trailing edge, and its energy is rapidly depleted due to single-photon resonant absorption. In case of curve *1* the perpendicular mode has less energy than the parallel

mode. The absorption of energy of this mode due to single-photon resonance leads to a lower total energy loss of the probe field than in case of curve *2*. Next, on the curves *1* and *2* follow the sections corresponding to the propagation of the parallel normal mode in conditions of EIT phenomenon. In these areas, the energy losses of both modes are negligible. Finally, at $s > 800$, these modes fall into the area of inefficiency of EIT phenomenon, and their energy is rapidly absorbed by the medium.

Note that sequential accounting of relaxation processes is usually carried out using equations for the elements of the density matrix with the times of transverse and longitudinal relaxation introduced in them. This approach is justified only in cases where relaxation processes are random Markov-type processes, i.e. processes without a probabilistic aftereffect. This situation occurs only if the energy levels of different states are sufficiently far apart [30]. In case of degeneration of energy levels, this condition is apparently not fulfilled. More general methods of accounting for relaxation processes [30,31] leads to an excessive complication of the mathematical model of the phenomenon under study. Therefore, we used Schrodinger equation with phenomenologically introduced relaxation terms to describe the response of the medium to electromagnetic radiation.

It should be noted that under EIT conditions, relaxation processes generally do not significantly affect the evolution of probe radiation in the medium [1–3]. This fact is confirmed in our case by a rather small difference between the curve *1* in Fig. 7 and the dashed curve obtained in calculation without taking into account relaxation processes.

In our work, the values a_{l0}, $l = 1, 2$ were modeled by inverse hyperbolic cosines. The application of other functions in boundary conditions (3) does not change the qualitative characteristics of EIT phenomenon. However, some quantitative characteristics of this process may vary. Thus, when using Gaussian function describing a pulse of the same duration to describe the value a_{20}, the penetration depth of the probe radiation into the medium is slightly diminished. This is because the values of Gaussian function decrease faster on the trailing edge than on the trailing edge of the inverse hyperbolic cosine.

Conclusion

The EIT process in fields of elliptically polarized pulses interacting with a Λ-scheme of degenerate quantum transitions is considered. It is assumed that the input pulse of the probe radiation has a significantly shorter duration than the input pulse of the control field, and both pulses simultaneously reach their peak value. It is shown that in a medium, a pulse of probe radiation can be represented as the sum of two normal modes — pulses propagating independently of each other at different speeds. PE normal modes have equal modulus but opposite sign compression parameters PE. The angle of inclination of the main axis of PE of one of the modes (parallel mode) is parallel to the main axis of PE control pulse, and the other mode (perpendicular mode) — perpendicular to the main axis of PE of the control pulse. The corresponding properties of modes are determined by the phenomenon of EIT.

The pulse of the parallel mode propagates faster than the pulse of the perpendicular mode, while the modes propagation speed is significantly less than the propagation of the control pulse in the medium. After passing a certain distance in the medium, the pulse of the perpendicular mode appears in the region of the trailing edge of the control pulse, where the intensity of the control field is insufficient for the effective occurrence of EIT phenomenon. In this region, the phenomenon of single-photon resonance leads to rapid attenuation of the perpendicular mode. The same situation also takes place with parallel mode. However, due to higher propagation speed, this mode passes through a medium with a much greater distance than the perpendicular normal mode before its disappearance.

Conflict of interest

The author declares that he has no conflict of interest.

References

[1] S.E. Harris. Phys. Today, **50** (6), 36 (1997).
[2] M.D. Lukin. Rev. Mod. Phys., **75** (2), 457 (2003).
[3] M. Fleischhauer, A. Imamoğlu, J.P. Marangos. Rev. Mod. Phys., **77** (2), 633 (2005).
[4] L.-M. Duan, M.D. Lukin, J.I. Cirac, P. Zoller. Nature (London), **414**, 413 (2001).
[5] A. Sinatra. Phys. Rev. Lett., **97** (25), 253601 (2006).
[6] M. Martinalli, P. Valente, H. Failache, D. Felinto, L.S. Cruz, P. Nussenzveig, A. Lezama. Phys. Rev., A, **69** (4), 043809 (2004).
[7] A. Godone, S. Micallilizio, F. Levi. Phys. Rev. A, **66** (6), 063807 (2002).
[8] M.D. Lukin, A. Imamoğlu. Nature (London), **413**, 273 (2001).
[9] S.E. Harris. Phys. Lett., **62** (9), 1033 (1989).
[10] H.H. Jen, Daw-Wei Wang. Phys. Rev. A, **87** (6), 061802(R) (2013).
[11] C. Basler, J. Grzesiak, H. Helm. Phys. Rev. A, **92** (1), 013809 (2015).
[12] R. Liu, T. Liu, Yi. Wang, Yu. Li, B. Gai. Phys. Rev. A, **96** (5), 053823 (2017).
[13] F. Le Kien, A. Rauschenbeutel. Phys. Rev. A, **91** (5), 053847 (2015).
[14] H.-H. Wang, J. Wang, Z.-H. Kang, L. Wang, J.-Yu. Gao, Yi. Chen, Xi.-J. Zhang. Phys. Rev. A, **100** (2), 013822 (2019).
[15] H. Li, Zh. Xu, H. Wang, J. Chen. Opt. Quant. Electron., **55**, Article № 198 (2023). DOI: 10.1007/s11082-022-04472-3
[16] H. Zheng, Yu. Zheng, M. Ouyang, H. Fan, Q. Dai, H. Liu, L. Wu. Opt. Express, **32** (5/26), 7318 (2024). DOI: 10.1364/OE.517111
[17] S. Wielandy, A.L. Gaeta. Phys Rev. Lett., **81**, 3359 (1998).
[18] Bo Wang, Sh. Li, J. Ma, H. Wang, K.C. Peng, M. Xiao. Phys. Rev. A, **73**, 051801(R) (2006).

[19] G.S. Agarwal, S. Dosgupta. Phys. Rev. A, **67**, 023814 (2003).
[20] V.A. Sautenkov, Y.V. Rostovtsev, H. Chen, P. Hsu, G.S. Agarwal, M.O. Scully. Phys. Rev. Lett., **94**, 233601 (2005).
[21] T.H. Yoon, Ch.Y. Park, S.J. Park. Phys. Rev. A, **70**, 061803(R) (2004).
[22] Z. Kis, G. Demeter, J.J. Janszky. Opt. Soc. Am. B, **30**, 829 (2013).
[23] O.M. Parshkov. Quant. Electron., **48** (11), 1027 (2018). DOI: 10.1070/QEL16683
[24] O.M. Parshkov. Quant. Electron., **49** (11), 1019 (2019).
[25] M. Jain, A. Kasapi, G.Y. Yin. Phys. Rev. Lett., **75**, 4385 (1995).
[26] A. Kasapi, M. Jain, G.Y. Yin, S.E. Harris. Phys. Rev. Lett., **74**, 2447 (1995).
[27] B.E.A. Saleh, M.C. Teich. *Fundamentals of photonics,* 2th ed. (Wiley-Interscience, 2007)
[28] R.L. deZafra, A. Marshall. Phys. Rev., **170** (1), 28 (1968).
[29] I.S. Grigoryev, E.Z. Mejlikhov (red.). *Fizicheskie velichiny, Spravochnik.* (Energoatomizdat, M., 1991) (in Russian).
[30] V.M. Fain. *Kvantovaya radiofizika. Fotoni i nelineiniye sredi* (Sovetskoye radio, M., 1972), v. 1. (in Russian)
[31] M.O. Scully, M.S. Zubairy. *Quantum Optics* (University Press, Cambridge 1997)

Translated by T.Zorina